Increasing Solubility and Stability of Linear Tricobalt(II) Chains with depa (Diethyldipyridylamide) Ligands

ARTICLE *in* INORGANIC CHEMISTRY · AUGUST 2003

Impact Factor: 4.76 · DOI: 10.1021/ic034149y · Source: PubMed

4 AUTHORS, INCLUDING:

John F Berry
University of Wisconsin–Madison
100 PUBLICATIONS **2,561** CITATIONS

Inorg. Chem. **2003**, *42*, 4425–4430

Increasing Solubility and Stability of Linear Tricobalt(II) Chains with depa (Diethyldipyridylamide) Ligands

John F. Berry,[†] F. Albert Cotton,*[,†] Tongbu Lu,[†,‡] and Carlos A. Murillo*[,†]

Department of Chemistry and Laboratory for Molecular Structure and Bonding, PO Box 30012, Texas A&M University, College Station, Texas 77842-3012, and School of Chemistry & Chemical Engineering, Sun Yat-Sen University, Guangzhou 510275, P. R. China

Received February 12, 2003

A new and more basic ligand has been used to make two new tricobalt extended metal atom chains (EMACs), namely, $Co_3(depa)_4Cl_2$, **3**, and $Co_3(depa)_4(CN)_2$, **4**. The depa ligand is di(4-ethyl-2-pyridyl)amide, a useful modification of the well-known di(2-pyridyl)amide, dpa, ligand. The new compounds have been thoroughly characterized, and informative comparisons are made of **3** with $Co_3(dpa)_4Cl_2$, **1**, and **4** with $Co_3(dpa)_4(CN)_2$, **2**, which were described several years ago. Introduction of the eight ethyl groups into the trimetal compounds improves solubility, makes oxidations easier, and allows for a more complete examination of the magnetic susceptibility as a function of temperature for **3** than was possible for **1**. The data clearly indicate that the upper state for **3** has $S = {}^3/_2$ and suggest that this is the case for **1** as well.

1. Introduction

As a first step in improving the solubilities and stabilities of extended metal atom chain (EMAC) compounds, we have recently reported the ligands etpda and depa (Chart 1) and their use to make pentanickel and trinickel compounds.[1,2] We considered it worthwhile to apply these ligands to the preparation of analogues of dpa and tpda EMACs of other metals. The extraordinary behavior of $Co_3(dpa)_4Cl_2$ (**1**), which has symmetrical and unsymmetrical chains, as well as other tricobalt EMAC compounds,[3−11] especially $Co_3(dpa)_4(CN)_2$ (**2**),[7] suggested that it would be particularly interesting to look at the properties of $Co_3(depa)_4X_2$ and $Co_5(etpda)_4X_2$ compounds. We report here the preparation and properties of two such compounds, $Co_3(depa)_4Cl_2$ (**3**) and $Co_3(depa)_4(CN)_2$ (**4**), which are analogues of **1** and **2**, respectively; $Co_5(etpda)_4Cl_2$ will be reported later.

Chart 1

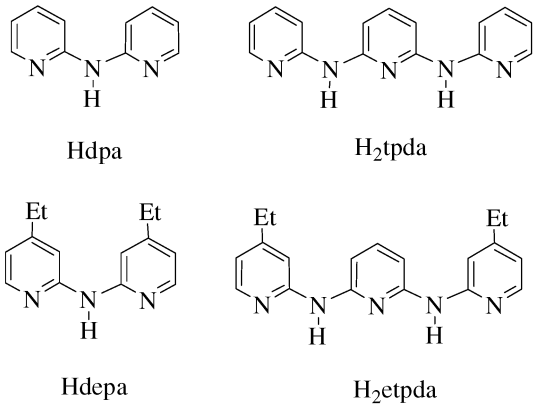

2. Experimental Section

Materials. 4-Ethylpyridine, sodium amide, and sodium cyanide were purchased from Aldrich. Anhydrous $CoCl_2$ was purchased from Strem Chemicals and was heated in thionyl chloride prior to use. Methyllithium (1.6 M in Et_2O) was purchased from Acros. Hdepa was prepared as previously described.[2] All solvents were

* To whom correspondence should be addressed. E-mail: cotton@tamu.edu (F.A.C.), murillo@tamu.edu (C.A.M.).
† Texas A&M University.
‡ Sun Yat-Sen University.

(1) Berry, J. F.; Cotton, F. A.; Lei, P.; Lu, T.; Murillo, C. A. *Inorg. Chem.* **2003**, *42*, 3534.
(2) Berry, J. F.; Cotton, F. A.; Lu, T.; Murillo, C. A.; Wang, X. *Inorg. Chem.* **2003**, *42*, 3595.
(3) Cotton, F. A.; Murillo, C. A.; Wang, X. *J. Chem. Soc., Dalton Trans.* **1999**, 3227.
(4) Cotton, F. A.; Murillo, C. A.; Wang, X. *Inorg. Chem.* **1999**, *38*, 6294.
(5) Clérac, R.; Cotton, F. A.; Daniels, L. M.; Dunbar, K. R.; Kirschbaum, K.; Murillo, C. A.; Pinkerton, A. A.; Schultz, A. J.; Wang, X. *J. Am. Chem. Soc.* **2000**, *122*, 6226.
(6) Clérac, R.; Cotton, F. A.; Daniels, L. M.; Dunbar, K. R.; Murillo, C. A.; Wang, X. *J. Chem. Soc., Dalton Trans.* **2001**, 386.
(7) Clérac, R.; Cotton, F. A.; Jeffery, S. P.; Murillo, C. A.; Wang, X. *Inorg. Chem.* **2001**, *40*, 1265.
(8) Clérac, R.; Cotton, F. A.; Dunbar, K. R.; Lu, T.; Murillo, C. A.; Wang, X. *Inorg. Chem.* **2000**, *39*, 3065.
(9) Clérac, R.; Cotton, F. A.; Dunbar, K. R.; Lu, T.; Murillo, C. A.; Wang, X. *J. Am. Chem. Soc.* **2000**, *122*, 2272.
(10) Clérac, R.; Cotton, F. A.; Daniels, L. M.; Murillo, C. A.; Wang, X. *Inorg. Chem.* **2001**, *40*, 1256.
(11) Yang, E.-C.; Cheng, M.-C.; Tsai, M.-S.; Peng, S.-M. *Chem. Commun.* **1994**, 2377.

10.1021/ic034149y CCC: $25.00
Published on Web 06/13/2003

Table 1. Crystallographic Data for **3** and **4** in Various Crystalline Forms at Different Temperatures

compound	**3**	**3**·0.5hexane	**3**·0.5hexane	**3**·acetone	**3**·$4CH_2Cl_2$·$2H_2O$	**4**·0.5hexane	**4**·$4CH_2Cl_2$·$2H_2O$
formula	$C_{56}H_{64}Cl_2Co_3N_{12}$	$C_{59}H_{71}Cl_2Co_3N_{12}$	$C_{59}H_{71}Cl_2Co_3N_{12}$	$C_{59}H_{70}Cl_2Co_3N_{12}O$	$C_{60}H_{76}Cl_{10}Co_3N_{12}O_2$	$C_{61}H_{71}Co_3N_{14}$	$C_{62}H_{76}Cl_8Co_3N_{14}O_2$
FW	1152.88	1195.97	1195.97	1210.96	1528.62	1177.11	1509.76
crystal system	tetragonal	tetragonal	tetragonal	tetragonal	tetragonal	tetragonal	tetragonal
space group	$P\bar{4}n2$	$P\bar{4}n2$	$P\bar{4}n2$	$P\bar{4}n2$	$I\bar{4}c2$	$P\bar{4}n2$	$I\bar{4}c2$
temp, K	213	213	297	213	213	213	213
a, Å	19.0972(7)	19.0498(5)	19.1585(4)	18.9312(11)	17.8664(8)	18.8948(8)	17.9117(7)
c, Å	15.8345(11)	15.8890(9)	15.9611(6)	16.0450(13)	21.900(2)	16.2414(13)	21.9213(17)
V, Å^3	5774.9(5)	5766.0(4)	5858.5(3)	5750.4(7)	6990.8(8)	5798.4(6)	7033.0(7)
Z	4	4	4	4	4	4	4
d(calcd), g cm$^{!3}$	1.326	1.378	1.356	1.399	1.452	1.348	1.426
R1[a], wR2[b] ($I > 2\sigma I$)	0.0490, 0.1504	0.0372, 0.0974	0.0413, 0.1054	0.0605, 0.1341	0.0646, 0.1744	0.0313, 0.0840	0.0536, 0.1473
R1[a], wR2[b](all data)	0.0569, 0.1643	0.0476, 0.1045	0.0629, 0.1232	0.0976, 0.1449	0.0754, 0.1977	0.0371, 0.0898	0.0615, 0.1600

[a] $R1 = \sum||F_o| - |F_c||/\sum|F_o|$. [b] $wR2 = [\sum[w(F_o^2 - F_c^2)^2]/\sum[w(F_o^2)^2]]^{1/2}$, $w = 1/\sigma^2(F_o^2) + (aP)^2 + bP$, where $P = [\max(0 \text{ or } F_o^2) + 2(F_c^2)]/3$.

dried and distilled under N_2 following standard procedures. All reactions were carried out under nitrogen with the use of standard Schlenk techniques.

Physical Measurements. Elemental analyses were performed by Canadian Microanalytical Services in British Columbia, Canada. The IR spectra were recorded on a Perkin-Elmer 16PC FT-IR spectrophotometer using KBr pellets. Cyclic voltammograms (CVs) and differential pulse voltammograms (DPVs) of the complexes (0.5 mM in CH_2Cl_2) were recorded on a BAS 100 electrochemical analyzer with $Bu^n_4NPF_6$ (0.1 M) electrolyte, Pt working and auxiliary electrodes, an Ag/AgCl reference electrode, a scan rate of 100 mV/s for the CVs, and a pulse width of 0.05 V for the DPVs. The magnetic susceptibility data were collected on a Quantum Design SQUID magnetometer MPMS-XL at a field of 1000 G on finely divided vacuum-dried samples. The temperature ranges were 2−400 K and 2−300 K for **3** and **4**, respectively. The data were corrected for diamagnetism calculated from Pascal's constants.

$Co_3(depa)_4Cl_2$, 3. Hdepa (0.454 g, 2.00 mmol) was dissolved in 20 mL of THF. The solution was cooled in a dry ice bath, and 1.3 mL of 1.6 M $LiCH_3$ in Et_2O (2.08 mmol) was added slowly. The solution, which turned yellow as it was allowed to warm to room temperature, was then transferred via cannula to a reaction flask containing anhydrous $CoCl_2$ (0.195 g, 1.50 mmol). The mixture was stirred at room temperature for 1 h and then refluxed for 16 h, giving a deep red-brown solution. The solvent was removed under vacuum, the remaining brown solid was extracted with toluene (2 × 8 mL), and the extract was then layered with hexanes. After 1 week, a large crop of deep brown crystals of $Co_3(depa)_4Cl_2$·$0.5C_6H_{14}$ had formed. The crystals were collected, washed with hexanes several times, and dried under vacuum. Yield: 0.17 g, 32%. Anal. Calcd for $C_{59}Cl_2Co_3H_{71}N_{12}$ [$Co_3(depa)_4Cl_2$·$0.5C_6H_{14}$]: C, 59.25; H, 5.94; N, 14.06%. Found: C, 59.34; H, 5.78; N, 14.01%. IR (KBr, cm^{-1}): 3448 (br, m), 3061 (w), 2965 (s), 2928 (m), 2868 (m), 1610 (vs), 1532 (s), 1473 (vs), 1423 (vs), 1293 (s), 1228 (m), 1179 (s), 1128 (w), 1061 (m), 1018 (s), 934 (s), 810 (s), 737 (m), 653 (w), 547 (m), 447 (s). ^{1}H NMR ($CDCl_3$, 300 MHz): δ 36.84 (s, 8H), 25.03 (s, 8H), 11.60 (s, 8H), 4.39 (t, J = 7.2 Hz, 24H), 3.73−3.66 (q, J = 7.2 Hz, 8H), 3.53−3.46 (q, J = 7.2 Hz, 8H).

$Co_3(depa)_4(CN)_2$, 4. A flask containing $Co_3(depa)_4Cl_2$ (0.21 g, 0.18 mmol) and NaCN (0.34 g, 6.9 mmol) was charged with 20 mL of acetone and 10 mL of methanol. The resulting mixture was stirred at room temperature for 16 h to give a red-brown solution. The solvents were evaporated under vacuum, the remaining solid was extracted with toluene (2 × 10 mL), and this solution was then layered with hexanes. After 1 week, dark brown crystals of $Co_3(depa)_4(CN)_2$·$0.5C_6H_{14}$ had formed. The crystals were collected, washed with hexanes, and dried under vacuum. Yield: 0.16 g, 78%. Anal. Calcd for $C_{61}Co_3H_{71}N_{14}$ [$Co_3(depa)_4(CN)_2$·$0.5C_6H_{14}$]: C, 62.24; H, 6.03; N, 16.66%. Found: C, 62.53; H, 6.18; N, 16.67%. IR (KBr, cm^{-1}): 3447 (br, s), 2965 (m), 2920 (m), 2868 (w), 2374 (w), 2092 (w), 1611 (vs), 1531 (m), 1428 (vs), 1292 (w), 1228 (w), 1179 (m), 1061 (m), 1018 (m), 933 (w), 807 (s), 733 (w), 652 (w), 549 (w), 455 (w).

X-ray Crystallography. Each crystal was mounted on the tip of a quartz fiber with a small amount of silicone grease and transferred to a goniometer head for data collection. X-ray diffraction data were collected on a Bruker SMART 1000 CCD area detector system at 213 K. Data were corrected for Lorentz and polarization effects using the program SAINTPLUS.[12] Absorption corrections were applied using SADABS.[13] The structures were solved by direct methods, which yielded the positions of all non-hydrogen atoms. These positions were refined first isotropically and then anisotropically. Some of the ethyl groups and hexane solvent molecules in **3** and **4** were disordered. All hydrogen atoms were placed in calculated positions during the final refinement cycles. All calculations were performed using the SHELXTL-97 programs.[14] The crystallographic data are listed in Table 1.

Compound **3** was obtained in several crystalline forms: **3** (with no interstitial solvent), **3**·0.5hexane, **3**·acetone, and **3**·$4CH_2Cl_2$·$2H_2O$. The first three crystallized isomorphously in space group $P\bar{4}n2$ (#118) with $Z = 4$, whereas the last formed crystals in $I\bar{4}c2$ (#120). In the case of **3**·0.5hexane, data were collected at both 213 and 297 K, and the molecule was found to lie on a *g* position and has a crystallographic 2-fold axis. In the latter, it lies on a *d* position with 222 symmetry. The best refinement of the **3**·0.5hexane structure was obtained at 213 K, and it has Co−Co = 2.3609(5) Å and Co−Cl = 2.413(1) Å. For the purpose of comparing the structures of **1** and **3**, however, it is important to use results that were obtained at the same temperature. Therefore, we use in Table 2 and for discussion the results for **3**·0.5hexane at 297 K, since the best data in the literature for **1** are at 296 K.

Figure 1 shows a side view of the $Co_3(depa)_4Cl_2$ molecule, and Figure 2 shows an end view of the $Co_3(depa)_4(CN)_2$ molecule. It is worth mentioning that, upon layering a toluene, THF, or diethyl ether solution of **3** with the commercial mixture of isomeric hexanes, only **3**·0.5*n*-hexane is crystallized; the packing diagram is shown in Figure 3. The *n*-hexane molecules are encapsulated inside

(12) *SAINTPLUS, V 5.00 Software for the CCD Detector System*; Bruker Analytical X-ray System, Inc.; Madison, WI, 1998. Absorption corrections were applied using SADABS.
(13) *SADABS*. Program for absorption correction using SMART CCD data based on the method of Blessing: Blessing, R. H. *Acta Crystallogr.* **1995**, *A51*, 33.
(14) Sheldrick, G. M. *SHELXTL97*; University of Göttingen, Göttingen, Germany, 1997.

Table 2. Comparison of *s*-$Co_3(dpa)_4Cl_2$ (**1**) and $Co_3(dpa)_4(CN)_2$ (**2**) with the New Isomorphous $Co_3(depa)_4X_2$ Compounds; X = Cl (**3**) and X = CN (**4**)

	1 (297 K)[5]	**2** (213 K)[7]	**3** (297 K)	**4** (213 K)
Co−Co	2.3369(4)	2.3392(2)	2.3787(7)	2.3371(4)
Co−N(end)	1.997(12)	1.982(12)	2.043(4)	1.992(2)
Co−N(ctr)	1.906(4)	1.904(3)	1.913(5)	1.897(3)
Co−X	2.448(8)	2.040(2)	2.3916(14)	2.025(2)
torsion ∠	46.9	47.0	50.2	49.3

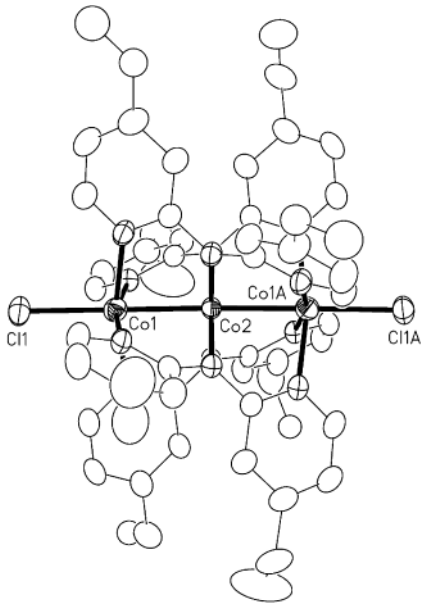

Figure 1. Thermal ellipsoid plot of **3** from **3**·0.5hexane at 297 K. Ellipsoids are drawn at 30% probability; only one orientation of the disordered ethyl groups is shown, and hydrogen atoms are omitted for clarity.

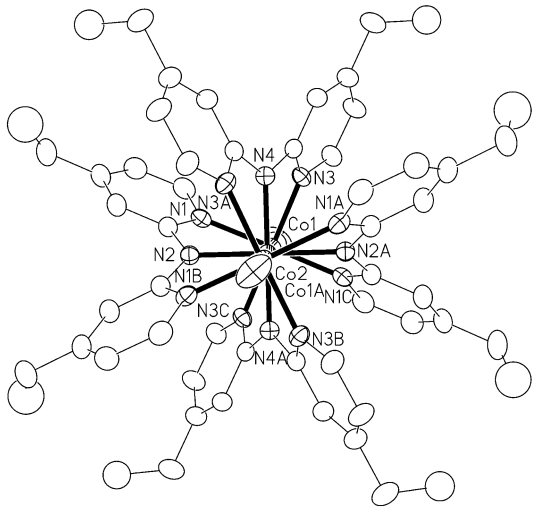

Figure 2. Thermal ellipsoid plot of **4** from **4**·$4CH_2Cl_2$·$2H_2O$ viewed along the Co_3 axis. Ellipsoids are drawn at 30% probability. Only one orientation of the disordered ethyl groups is shown, and hydrogen atoms have been omitted for clarity.

small channels in the structure and do not leave the crystals even when they are placed under dynamic vacuum overnight. For **3**·acetone, the acetone molecules also reside in these channels. Layering a toluene solution of **3** with cyclohexane produced **3** without interstitial solvent. Interestingly, the same packing occurs as shown in Figure 3, but the interstitial channels are empty. Therefore, the encapsulation of *n*-hexane appears to be very selective.

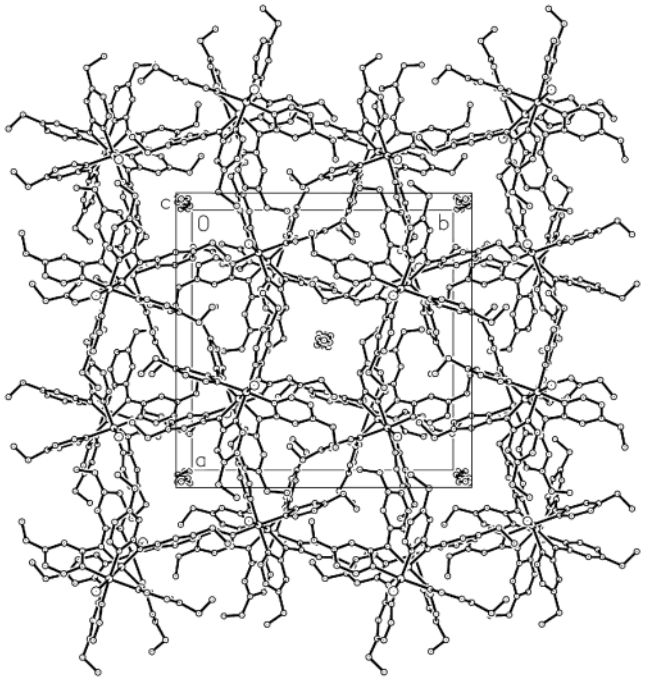

Figure 3. Packing diagram of **3** from **3**·0.5hexane at 297 K showing the narrow channels at 0 0 *z* and $^1/_2{}^1/_2$ *z* filled with encapsulated *n*-hexane molecules.

3. Results and Discussion

It is worth emphasizing that, just as **1** and **2** form isomorphous crystals with CH_2Cl_2 solvent, so also do **3** and **4** with hexane. Thus, the well-established notion that, from a molecular packing standpoint, Cl and CN ligands are commonly equivalent is valid here.

Comparison of 1 and 3. The structure of **3** shown in Figure 1 with the dimensions listed in Table 2 is representative of all crystal forms and bears a strong resemblance to that of the symmetrical form of **1**, *s*-$Co_3(dpa)_4Cl_2$. Molecular dimensions are compared in Table 2. Although we have not made an exhaustive effort (since trying to prove a negative is unrewarding and usually unsuccessful), we cannot say for certain that no unsymmetrical form of **3**, i.e., corresponding to *u*-$Co_3(dpa)_4Cl_2$, exists, but we have found no evidence of such product when **3** is isolated in crystalline form. The ^{1}H NMR spectrum of **3** shows D_4 symmetry in solution and is qualitatively similar to that of **1**, except for the replacement of one of the four ring-proton signals by new ones due to the ethyl groups. Because the magnetic properties of **1** and **3** (vide infra) are quantitatively different, however, and also because a different solvent was used, the chemical shift values are correspondingly different.

It must be noted, however, that the structures of **1** and **3** differ more than we had anticipated. In **3**, the Co−Co bonds are 0.042(1) Å longer, and the Co−Cl distances are 0.06(1) Å shorter than the corresponding bonds in **1**. Both differences are, in a statistical sense, quite real, i.e., 42 times and 6 times σ, respectively. The differences do not, however, contradict our premise, established for the Ni_3[2] and Ni_5[1] compounds, that ethyl groups on the outer pyridyl groups do not qualitatively alter the nature of the EMACs (i.e., whether they are expected to serve as molecular conductors or

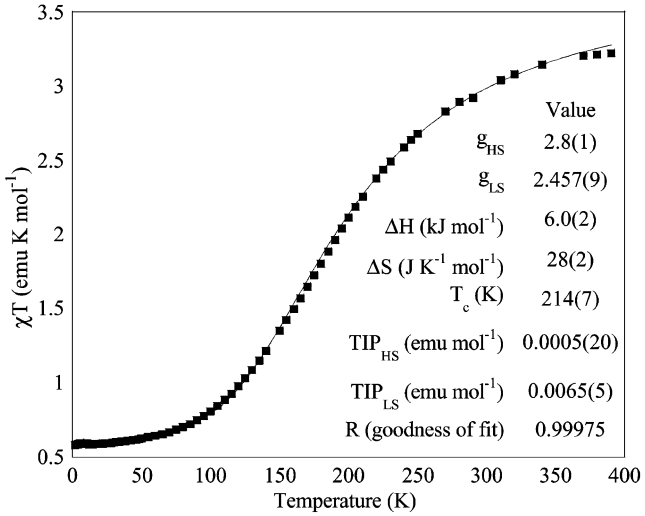

Figure 4. Plot of χT vs T for **3**. The solid line represents the best theoretical fit of the curve (see text).

insulators). The lengths of the Co−N bonds and the torsion angle do not change significantly from **1** to **3**.

The magnetic properties of *s*-$Co_3(dpa)_4Cl_2$ (**1**) were previously studied in considerable detail. It was found that there is a ground state with $S = {}^1/_2$, $\chi T = 0.536$ emu·K/mol, and $g = 2.38(2)$, which appears as a plateau in the χT vs T curve up to about 160 K. Similarly, **3** is found (Figure 4) to have a ground state with $S = {}^1/_2$, $\chi T = 0.566$ emu·K/mol, and (according to the best fit for the entire χT vs T curve) $g = 2.457(9)$. For **1**, χT increased from 160 to 350 K in a manner typical for a spin-crossover process, but nothing approaching an asymptotic limit could be reached before decomposition. We examined the ability of both $S = {}^3/_2$ and $S = {}^5/_2$ upper states to fit the data and found it impossible to come to a sure conclusion about which state was the correct upper state. For **3**, the value of χT levels off at ~3.2 emu·K/mol at 350 K, so it is clear that the upper state has $S = {}^3/_2$. Because of this, in **3**, it is possible to fit the data for a complete spin-crossover process and determine independently the Landé factors for both the ground and upper states. The value for the $S = {}^3/_2$ state of 2.8(1) is not identical to that for the $S = {}^1/_2$ state, although the assumption that g is the same for both had to be made in the case of **1** because so little of the upper state was represented in the available susceptibility data. Indeed, the fact that g can be greater for the upper $S = {}^3/_2$ state renders the idea that the upper state for **1** could have $S = {}^5/_2$ much less likely. As can be seen in Figure 4, the fit to the $S = {}^1/_2 \rightarrow S = {}^3/_2$ model with two different g values is excellent ($R = 0.9998$) for **3**.[15]

If **1** undergoes an $S = {}^1/_2$ to $S = {}^3/_2$ spin-crossover process as **3** does, it is also useful to compare the thermodynamic data (as derived from the magnetic susceptibility curves) of these spin equilibria. For **1**, the relevant values are $\Delta H = 18.0$ kJ/mol, $\Delta S = 54.7$ J·K^{-1}·mol^{-1}, and $T_c = \Delta H/\Delta S = 468$ K.

The corresponding values for **3** are listed in Figure 4. The different values of T_c (i.e., more than 250 K greater for **1** than for **3**) are consistent with the main differences in the χT vs T curves for **1** and **3**, but it is also interesting to consider the enthalpy and entropy components individually. Although ΔS for **1** is more favorable than for **3**, ΔH for **1** is about 3 times that for **3**. Thus, the $S = {}^3/_2$ state for **3** lies ~12 kJ/mol lower in energy than it does for **1**. It is interesting but a little surprising that such a seemingly minor change to the ligand should affect so much the relative energy of the high-spin state of the compound.

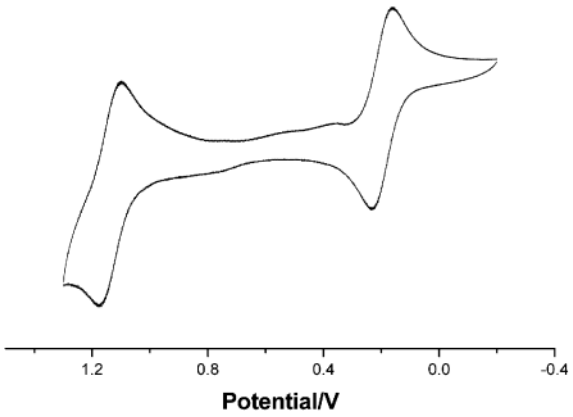

Figure 5. Cyclic voltammogram of **3** taken in CH_2Cl_2 with NBu_4PF_6 supporting electrolyte.

The final point of comparison between **1** and **3** to which we draw attention is the difference in oxidation potentials in solution. As previously observed for the corresponding Ni_3[2] and Ni_5[1] compounds, the introduction of the ethyl groups makes it significantly easier to oxidize **3** than it is to oxidize **1**. Thus, for **3**, as shown in Figure 5, there are reversible oxidations at 0.195 and 1.138 V, compared to those at 0.320 and 1.24 V reported for **1**. The greater basicity of the depa ligand is responsible for this change.

Comparison of 2 and 4. The structural similarity here is extremely close, as shown by the key dimensions in Table 2. Thus, no further comment is required.

Another comparison we have made for these two compounds concerns their oxidizability. Compound **4** shows two reversible oxidation waves at 0.101 and 0.863 V vs Ag/AgCl. The corresponding waves for **2** are at 0.276 and 1.008 V.

(15) The curve fit is based on the following model of the compound as an ideal solution of $S = {}^1/_2$ and $S = {}^3/_3$ entities:

$$\chi T = \frac{\left[\frac{g_{HS}^2}{4}C_{HS} + (TIP_{HS})T\right] - \left[\frac{g_{LS}^2}{4}C_{LS} + (TIP_{LS})T\right]}{1 + \exp\left[\frac{\Delta H}{R}\cdot\left(\frac{1}{T} - \frac{1}{T_c}\right)\right]} + \left[\frac{g_{LS}^2}{4}C_{LS} + (TIP_{LS})T\right]$$

where g_{HS} and g_{LS} are the Landé factors of the $S = {}^3/_2$ and $S = {}^1/_2$ states, respectively; C_{HS} and C_{LS} are the Curie constants for the $S = {}^3/_2$ and $S = {}^1/_2$ states, respectively; R is the gas constant; ΔH is the enthalpy; and T_c is the critical temperature (i.e., the temperature at which equimolar amounts of $S = {}^1/_2$ and $S = {}^3/_2$ compounds are present). Also given in Figures 4 and 6 are the derived values of $\Delta S = \Delta H/T_c$. Parameters for TIP_{HS} and TIP_{LS} (temperature-independent paramagnetism) for the $S = {}^1/_2$ and $S = {}^3/_2$ states, respectively, were introduced in the fitting of **3**. These parameters might affect the accuracy of the refined g values, but the impact of such a correction is not significant. The TIP for **3**, as well as the rather high g values, are likely due to spin−orbit coupling. The TIP_{LS} parameter refined for **4** was negligible ($<1 \times 10^{-6}$ emu/mol). Therefore, the equation used in the fitting of **4** shown in Figure 6 was modified by removal of the TIP parameters.

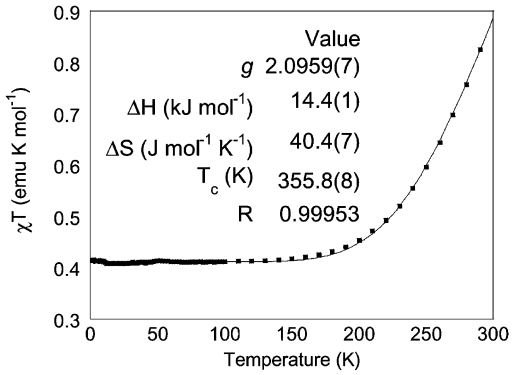

Figure 6. Plot of χT vs T for **4**. The solid line represents the best theoretical fit of the curve with least-squares parameters given in the inset.

Thus, again, the depa ligand gives significantly greater access to oxidized species, and in this case, it would appear that the $[Co_3(depa)_4X_2]^{2+}$ ion should be relatively easy to isolate by using a chemical oxidant such as $AgPF_6$ in CH_2Cl_2.

The magnetic susceptibility data for **4** (Figure 6) are surprisingly different from those for **3**. Whereas the upper $S = {}^3/_2$ state for **3** is 90% occupied at 350 K, essentially only the $S = {}^3/_2$ state for **4** is occupied up to 150 K, and then the $S = {}^3/_2$ state is only 29% populated at room temperature. The χT value for **4** at 300 K is only 0.9 emu·K/mol, whereas for **3**, it is above 2.5 emu·K/mol. Thus, in **4**, the spin equilibrium has been altered in such a way that either the $S = {}^1/_2$ state is highly stabilized or the $S = {}^3/_2$ state is highly destabilized.

To quantitatively determine the difference between **3** and **4**, the magnetic susceptibility data for **4** were modeled using the same method as used for **3**,[15] with the exception that only one value of g can be refined (because of the small population of the upper state). The results of the refinement are given in the inset to Figure 6.

Although ΔS for the $S = {}^1/_2 \rightarrow S = {}^3/_2$ process is more favorable for **4** than for **3**, ΔH is again the major factor in this equilibrium. The $S = {}^3/_2$ state for **4** lies ~8 kJ/mol higher in energy than it does for **3**. To understand why such a change in the magnetic properties of the compound can occur simply by substituting cyano ligands in place of chloro ligands, a basic molecular orbital approach that we have recently developed[16] is useful.

Theory[17] (density functional calculations) and experiment (the physical properties of $\mathbf{1}^+$) agree that the SOMO of the ground state of **1** is a Co_3 σ nonbonding orbital with significant Co−Cl antibonding character. Chart 2 shows that this arises from symmetry-matched interactions of the Cl^- lone pairs with the Co_3 σ_{nb} and σ^* orbitals, which lower the energy of the Co−Cl bonding orbitals and raise the energies of the Co_3 σ_{nb} and σ^* orbitals significantly. As cyanide ligands are generally considered better σ donor ligands than halide ions, the destabilizing interaction of CN^- with the SOMO and LUMO of the Co_3 chain is expected to be much more pronounced, leaving these orbitals much higher in energy than the other occupied Co_3 bonding orbitals.

Chart 2

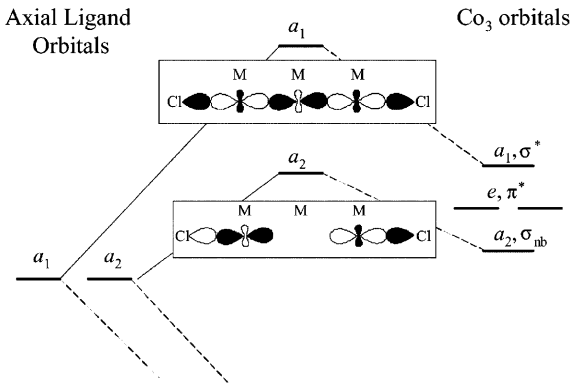

Chart 3

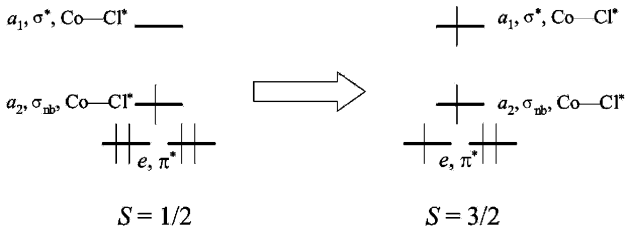

The σ^* orbital, however, must be used in the spin-crossover process, since it is the only cobalt-based orbital that is completely empty in the ground state. As shown in Chart 3, the spin-crossover process involves removal of an electron from a filled orbital of lower energy (e.g., the π^* orbital) and placing it in the σ^* orbital, resulting in the observed quartet state. A larger energy gap between the filled orbitals and the σ^* orbital would disfavor the spin crossover. Thus, as the σ^* orbital moves higher in energy with increasing axial donor strength, the spin-crossover process becomes less favorable. Such is the case in **3** and **4**, where the critical temperature (T_c) for the cyano complex is over 150 K greater than that for the chloro complex.

This is also seen in the magnetic susceptibility data for **1** and **2**, although a quantitative curve fit for **2** was not obtained. Whereas the spin equilibrium for **1** becomes apparent at just above 150 K, for **2**, only the $S = {}^1/_2$ state is populated up to 300 K.

These magnetic results are very significant because they show that, by subtle changes to either the bridging or axial ligands of the Co_3 chains, tuning of the magnetic properties of the compounds can be achieved.

4. Concluding Remarks

It is clear from this work that, even though the depa ligand is not quite as convenient to use because it has to be synthesized, it offers significant advantages over the commercially available dpa ligand. This was already clear for nickel compounds,[2] and it is now evident that it is likely to be true for all metals.

(16) Berry, J. F.; Cotton, F. A.; Daniels, L. M.; Murillo, C. A.; Wang, X. *Inorg. Chem.* **2003**, *42*, 2418.
(17) (a) Rohmer, M.-M.; Bénard, M. *J. Am. Chem. Soc.* **1998**, *120*, 9372. (b) Rohmer, M.-M.; Strich, A.; Bénard, M.; Malrieu, J.-P. *J. Am. Chem. Soc.* **2001**, *123*, 9126.

Acknowledgment. We thank the National Science Foundation, the NIRT (Nanoscale Science and Engineering, NIRT Grant DMR-0103455), and the Telecommunications and Information Task Force (TITF) at Texas A&M University. Dr. Xiaoping Wang provided much appreciated help with the structure determinations, and H. Sakiyama offered very helpful suggestions that improved the fitting of the magnetic data. J.F.B. is grateful to the National Science Foundation for a predoctoral fellowship.

Supporting Information Available: X-ray crystallographic data for **3, 3**·0.5hexane at 297 and 213 K, **3**·acetone, **3**·4CH_2Cl_2·2H_2O, **4**·0.5 hexane, and **4**·4CH_2Cl_2·2H_2O in CIF format. This material is available free of charge via the Internet at http://pubs.acs.org.

IC034149Y